The International Journal of Advanced Manufacturing Technology (2023) 125:4119–4131
https://doi.org/10.1007/s00170-023-11019-7

ORIGINAL ARTICLE

Controllable preparation of non-uniform tool edges by magnetorheological finishing

Xiangyu Guan[1] · Donghai Zhao[1] · Yaxin Yu[1,2] · Dunwen Zuo[3] · Shuquan Song[1]

Received: 30 August 2022 / Accepted: 28 January 2023 / Published online: 4 February 2023

Abstract
The cutting-edge radius plays a crucial role in precision machining. An optimally matched radius to the uncut chip thickness can significantly extend tool life. When the uncut chip thickness varies along the cutting edge, preparing the edge with individual radii at different positions is ideal. A novel non-uniform edge preparation approach based on magnetorheological finishing is proposed in this paper. The flexible abrasive tool formed by the magnetorheological effect is presented to prepare a controllable removal and low-damage cutting edge. In this study, the edge preparation device is designed and built, and the structure of the grinding basin is optimized. The magnetic induction intensity distribution in the grinding basin under the action of the external magnetic field is studied. Considering the influence of the magnetic induction intensity, the viscosity change rule of the magnetorheological fluid under different magnetic field intensities is discussed, and a flow field simulation model with variable viscosity is developed. Based on simulation and experiment, the cutting-edge material removal rate is analyzed, and the Preston coefficient is calculated. The results show that magnetorheological preparation can achieve non-uniform directional quantitative removal of edge materials. This study provides a new approach for preparing non-uniform tool edges, which has a positive significance in producing high-performance tools.

Keywords Precision machining · Cutting-edge preparation · Magnetorheological finishing · Non-uniform edge

1 Introduction

Edge radius is an important parameter used to describe the appearance of the tool edge. It affects cutting force, temperature, machining quality, and tool life [1–4]. Zhao et al. [5] found that the cutting-edge radius affects the surface roughness of AISI52100 steel in hard turning, and an edge radius of 30 μm showed better performance in terms of surface roughness. Hariprasad et al. [6] investigated the edge radius effect on end milling of TiAl6V4 under minimum quantity cooling lubrication conditions, and it was found that there is an optimal edge radius of around 48 μm for better machining results. Jiang et al. [7] optimized the geometric parameters of the cutting edge for the finishing machining of 30Cr alloy steel and concluded that the optimal cutting-edge radius is 14 μm. An et al. [8] conducted orthogonal cutting experiments using T700/LT03A UD-CFRP laminates, and the results showed that a cutting-edge radius of 15 μm helps obtain smaller cutting forces. It can be seen that the optimal cutting-edge radius is variable and it needs to be designed to match the machining conditions.

Cutting-edge preparation effectively changes the edge radius and turns the edge design scheme into a physical object. Scholars have researched tool edge preparation methods and techniques and developed various preparation processes [9–12]. Krebs et al. [13] demonstrated the feasibility of using wet abrasive jet machining to prepare micro milling tools and concluded that it significantly improves the edge performance. Wang et al. [14] studied the influence of cutting edges produced by pressurized air wet abrasive jet machining on cutting performance during orthogonal machining of AISI 4140, and proved that the pressurized air wet abrasive jet machining could prepare cutting edges of different shapes and sizes. Tiffe et al. [15]

✉ Shuquan Song
ssq@ycit.edu.cn

1 College of Mechanical Engineering, Yancheng Institute of Technology, Yancheng 224051, China

2 College of School of Medicine, Chemical and Materials Engineering, Taizhou University, Taizhou 318000, China

3 College of Mechanical and Electrical Engineering, Nanjing University of Aeronautics & Astronautics, Nanjing 210016, China

presented an approach to predict optimal cutting-edge microshapes in machining the nickel-base alloy Inconel 718. The cutting edges are prepared by pressurized air wet abrasive jet machining. Denkena et al. [16] concluded that the size of the cutting-edge radius could be adapted via the 5-axis brushing process. Malkorra et al. [17] macroscopically simulated the abrasive flow process of parts in drag finishing and concluded that the finishing efficiency is the highest when the included angle between parts and abrasives is 30° to 60°. Lv et al. [18] prepared cemented carbide end mills by drag finishing using four abrasives and concluded that the abrasive HSO 1/100 could produce high-quality edges with a maximum cutting-edge radius of 15 μm. Karpuschewski et al. [19] studied the influence of magneto-abrasive machining on the microgeometry of the cutting edges and showed that MAM could reproduce the defined radius of the cutting edges and improve the tool surface quality.

In-depth studies have shown a coupling between uncut chip thickness and tool edge radius, which can be used as a basis for tool edge optimization design. The cutting efficiency decreases significantly when the uncut chip thickness is less than twice the edge radius [20]. When the uncut chip thickness is less than 25% of the edge radius, no chip is formed in Ti6Al4V orthogonal cutting [21]. Therefore, there is an optimal ratio between the uncut chip thickness and the cutting-edge radius during machining. Finding the optimal ratio is the key to guiding the tool edge's design. However, the uncut chip thickness varies along the cutting edge in some machining processes. The thickness of the uncut chip gradually decreases in the vertical direction during the turning process [22]. During micro-end milling, the uncut chip thickness distribution is also not uniform [23]. The non-uniform distribution of undeformed chips along the cutting edge is particularly significant in hard whirling. When the uncut chip thickness is not uniformly distributed, the cutting-edge radius should vary with the uncut chip thickness to obtain the best cutting effect. Yussefian et al. [24] manufactured variable microgeometry (VMG) cutting tools in which the edge microgeometry varies along the edge line with respect to specific variables (such as machining parameters or expected tool wear) and showed that VMG tools improve significantly in terms of tool life and machined surface quality relative to conventional tools. Özel [25] presented experimental and FE modeling investigations of 3D turning using PcBN inserts and concluded that variable microgeometry insert edge designs significantly reduce heat generation and stress concentration along the cutting edge, contributing to improved tool life. Karpat et al. [26] performed cutting experiments and 3D finite element analysis to compare uniform and variable edge preparations. The results revealed that the variable edge preparation inserts perform better than uniform edge preparation counterparts if the variable edge is properly designed for the given cutting conditions. But, the cutting edge prepared by abrasive jet machining, drag finishing, and magneto-abrasive machining is uniform. Brushing can prepare non-uniform edges, and the manufacturing process is complicated.

This paper proposes a new approach based on magnetorheological finishing to prepare non-uniform cutting edges to meet the challenge of variable edge preparation. The magnetorheological preparation device is designed and built, and the structure of the grinding basin is optimized. After adding the rotating tool, a fluid model with variable viscosity is established to simulate the flow field in the grinding basin. The material removal efficiency and spatial distribution law of the edge radius are studied by analyzing the simulation and experimental results.

2 Magnetorheological preparation for cutting edge

2.1 Mechanism of magnetorheological preparation

Magnetorheological fluid (MR fluid) exhibits high viscosity and low fluidity with an applied magnetic field. The high-hardness abrasive particles are mixed into the MR fluid, and the Bingham fluid with cutting ability is formed under the action of the magnetic field. This high-viscosity fluid mixed with abrasive particles is identical to a flexible abrasive tool, which can be used to prepare cutting edges. As shown in Fig. 1, the cutting edge is placed horizontally in the magnetorheological preparation fluid. The abrasive particles are evenly distributed in the magnetorheological fluid without an external magnetic field. When a magnetic field is applied, the magnetic particles form a chain structure, and the abrasive particles gather on the surface of the magnetic particles to become a flexible abrasive tool. Through the forced flow of the MR fluid and the relative rotation of the tool, the grinding head produces a tangential cutting effect on the tool edge surface to remove the edge material. Due to the various relative velocities and pressures at different points on the tool edge, the material removal rate also varies. Therefore, it is theoretically possible to prepare a non-uniform edge using the magnetorheological preparation method shown in the figure, but the efficiency and distribution law of the edge material removal need to be further investigated.

2.2 Magnetorheological device for cutting-edge preparation

2.2.1 Overall design of the preparation device

To confirm the feasibility of magnetorheological preparation for cutting edges and reveal its material removal law,

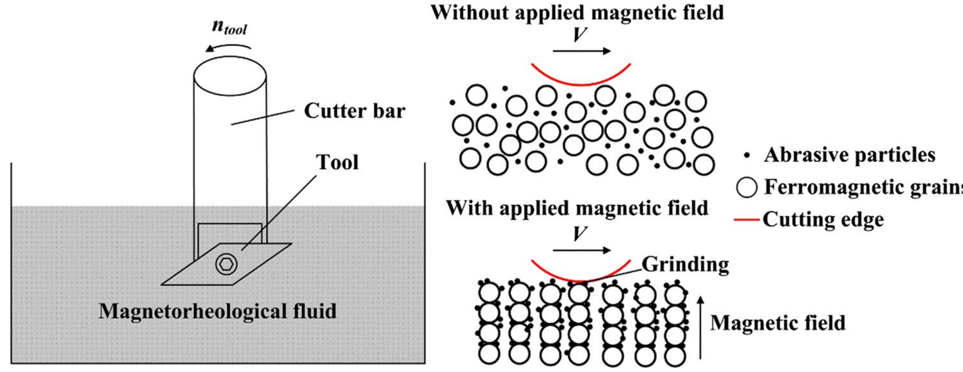

Fig. 1 Principle of magnetorheological preparation

a preparation device is designed in this study. The device consists of a tool clamping and driving part, a magnetorheological fluid circulation system, a magnetic field generation module, and a support structure. As shown in Fig. 2, the tool is installed at the end of the cutter bar, and the assembly of the rod and the shaft sleeve is connected with the motor output shaft at the upper end employing a plum blossom coupling. The controller can adjust the stepper motor speed and drive the tool to rotate at a rate of 0–6 r/s. Loosen the screw, and the rotating plate can be rotated along the U-shaped holes to adjust the installation angle of the tool. The support plate can be moved up or down along the adjustment holes

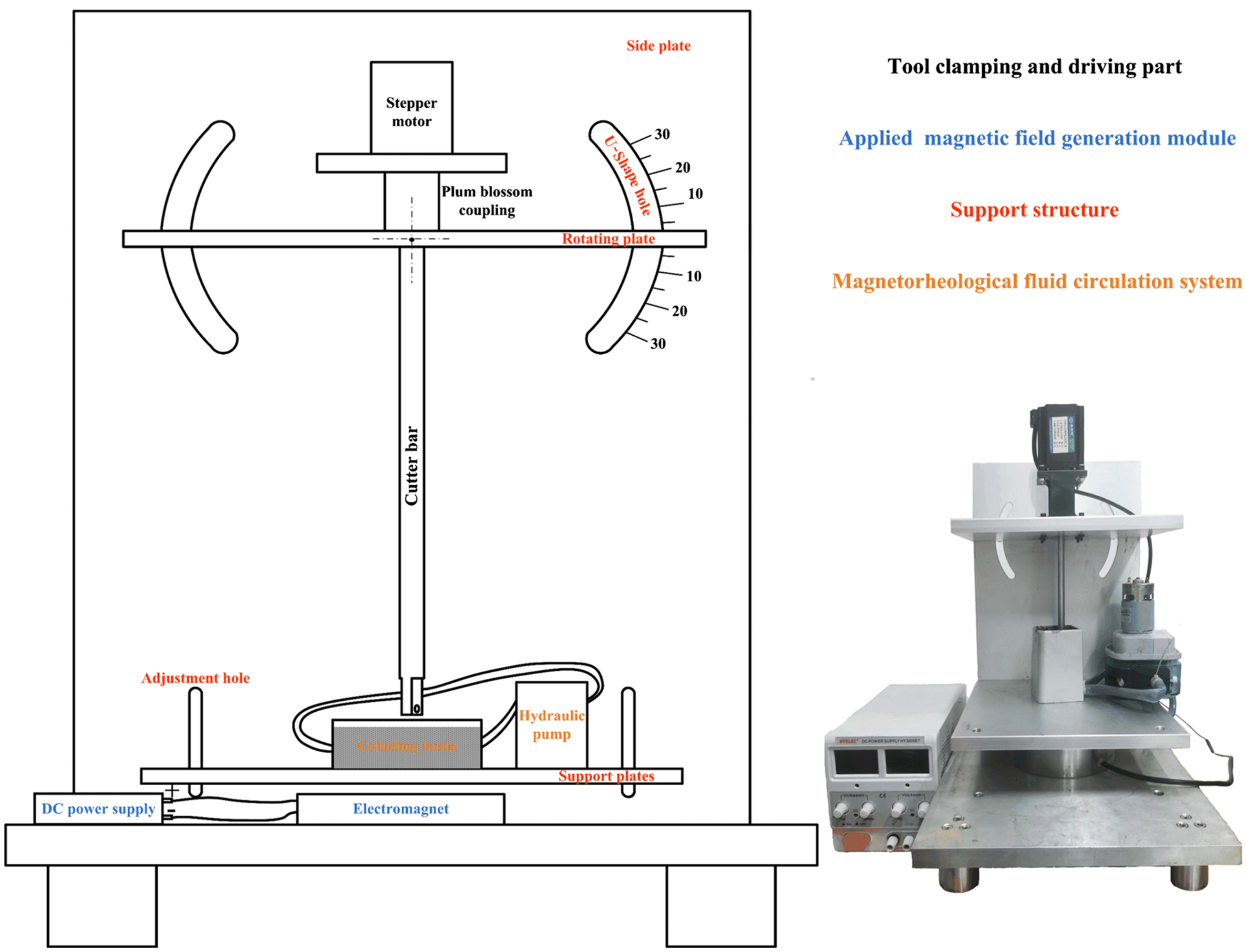

Fig. 2 Magnetorheological preparation device for cutting edge

to set the tool's immersion depth. The grinding basin holds the MR fluid; its outlet and inlet are connected with the hydraulic pump through hoses. An electromagnet XDW/140 provides the applied magnetic field under the basin. The magnetic induction intensity can be adjusted by changing the parameters of the DC power supply.

2.2.2 Structure optimization of the grinding basin

The grinding basin's shape will affect the MR fluid's flow characteristics and then affect the removal rate and distribution. To select the appropriate container shape, this paper simulates the flow field of the MR fluid in a square container with a fillet (SR), round container (R-type), and square container (S-type) using Fluent software. The speed inlet is set, the inlet speed is 10 m/s, the pressure outlet is set, the outlet pressure is 0 Pa, and the flow model is k-epsilon. The simulation results are shown in Fig. 3. The three kinds of containers have high flow velocities at the outlet and inlet.

The high-speed area at the outlet of SR and S-type containers is small, while the high-speed area at the outlet of R-type is large, and the high-speed area is connected with the inlet. The low-speed area of the S-type is large, and the inlet and outlet are separated, so the flow is insufficient. The zone with a low flow rate in the R-type is in the center, and the distribution range is the smallest. The overall flow rate is distributed radially, and the distribution level is obvious, conducive to the exchange of magnetorheological fluid, and the uniformity of the magnetorheological fluid in the preparation area is ensured.

According to the above analysis, the flow characteristics of a round container are better than those of the other two forms. Therefore, the round shape is selected as the shape of the grinding basin in this paper. On this basis, the inlet and outlet distribution is also studied. Three opening modes are chosen: the same side and same height opening (SS), the different side and same height opening (DS), and the different side and different height opening (DD). The simulation setting is the same as above, and the simulation results are shown in Fig. 4. The flow velocity gradually increases from the inside out, with a concentric distribution and low-velocity zone near the wall. When opening on different sides and heights, the zone of low flow rate (0–0.71 m/s) is the smallest, and the area of MR fluid with a high flow rate is the largest, with a small flow dead zone. Therefore, the grinding basin adopts a round shape and opens on different sides at different heights.

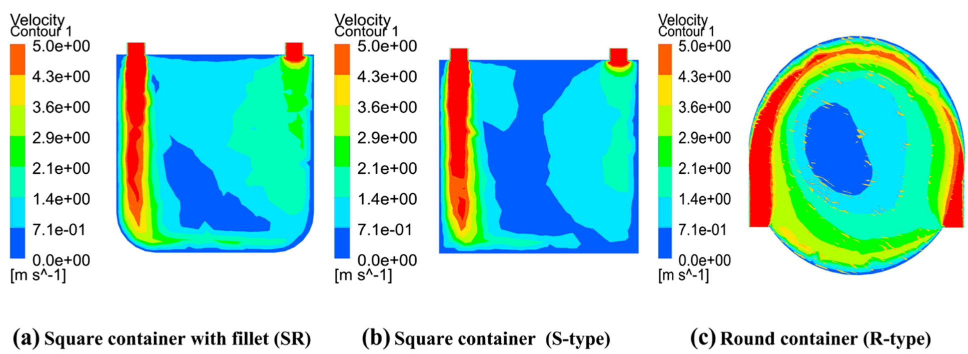

Fig. 3 Flow field analysis of containers with different shapes

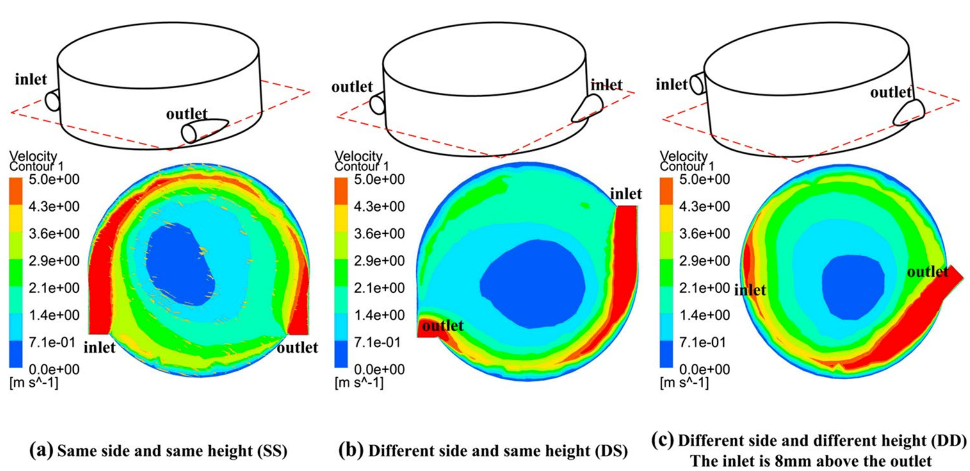

Fig. 4 Flow field analysis of round container with different openings

2.3 Material removal rate

The material removal effect of magnetorheological preparation can be expressed by the Preston equation as follows:

$$R = KPVT \tag{1}$$

where P is the pressure of the flexible grinding head on the workpiece surface, V is the relative velocity between the magnetorheological fluid and the workpiece surface, T is the preparation time, and K is the Preston coefficient related to the magnetorheological fluid and workpiece materials.

$$P = P_d + P_m \tag{2}$$

where P_d is the hydrodynamic pressure and P_m is the magnetization pressure of the magnetorheological fluid.

$$P_m = \mu_0 \int_0^H M_j dH \tag{3}$$

where μ_0 is vacuum permeability, M_f is magnetization, and H is magnetic field intensity.

Relative to P_d, the value of P_m is too small [27], so we can use the following formula to express the removal effect of magnetorheological preparation.

$$R = KP_d VT \tag{4}$$

When the magnetorheological fluid is unchanged and the preparation time is the same, the removal rate of the cutting-edge material is determined by the hydrodynamic pressure and the velocity. Flow field simulation can obtain these two values, and the relative material removal rate can be calculated.

The fluid viscosity is no longer uniform with the applied magnetic field due to the different magnetic field intensities at various points in the grinding basin. Assigning the same viscosity value to the fluid used for the simulation would be inappropriate. This paper first simulates the magnetic field to obtain the intensity distribution to establish an accurate viscosity distribution model. Then, the viscosity of the magnetorheological fluid under different magnetic field intensities is measured.

2.3.1 Electromagnetic field simulation

The viscosity of magnetorheological fluids varies with the magnetic induction intensity. The magnetic field generated by the circular DC electromagnet is consistent with the shape of the container, and the magnetic field strength of the electromagnet can be changed by adjusting the current. Therefore, this paper uses the circular electromagnet as the magnetic field generator. The current excitation is selected, and the total ampere-turn is 7750 N·A. The circular surface with a diameter of 200 mm is set as the insulation boundary condition, and the material is a vacuum. Table 1 shows the shape parameters of the electromagnet, and Table 2 shows the material parameters of the electromagnet. The Maxwell software is employed to simulate the magnetic field of the electromagnet.

2.3.2 Viscosity of the magnetorheological fluid

A TD8620 digital Gauss meter and viscometer were used to measure the viscosity of the magnetorheological preparation fluid under different magnetic field intensities. The container containing the magnetorheological fluid is placed over the electromagnet. Part of the rotor is submerged in the MR fluid, and the distance between the middle position of the submerged part and the magnet surface is h. The current of the DC power supply connected to the electromagnet is adjusted, the magnetic field strength in the center of the electromagnet is changed, and the magnetic induction intensity at the position h is measured at this time using the Gauss meter. Under a constant shear strain rate, the viscosity of the magnetorheological fluid under different magnetic field intensities can be obtained by a viscometer. The experimental parameters are shown in Table 3.

Table 1 Shape parameters of the electromagnet

Coil inner diameter (mm)	Coil outer diameter (mm)	Outer diameter of outer polar head (mm)	Inner diameter of outer polar head (mm)	Inner pole head diameter (mm)	Pole height (mm)
35	60	120	90	35	60

Table 2 Electromagnet material parameters

Coil material	Pole material	Iron core material
Copper	Q235	steel-1008

Table 3 Experimental data of viscosity measurement

Viscometer model	Shear rate (s-1)	Rotor
NDJ-1	200	4

3 Results and discussion

3.1 Simulation of the magnetic induction intensity

Using the electromagnet model parameters listed in Table 1 and Table 2, the magnetic induction intensity in the area of the grinding basin was simulated. Considering the influence of the magnetic induction intensity on the viscosity of the magnetorheological fluid and simplifying the problem, the magnetic field of the entire magnetorheological fluid is divided into five layers in the vertical direction. Starting from the inner side of the container bottom, each 3-mm thickness is divided into a layer. Figure 5 shows the magnetic induction intensity curves at the lower surface of each layer.

The magnetic field intensities of these surfaces have a substantially symmetrical "M"-shaped distribution. From the edge of the container to the center, the magnetic induction intensity first increases and then decreases, which is symmetrical about the axis. Its value reaches a maximum of approximately 35 mm from the center. On the surface with a height of 0 mm, the maximum value of the magnetic induction intensity is about 200 mT. The difference between the magnetic induction intensity at the center and the maximum value is the largest, about 110 mT. With increasing height, the peak of magnetic induction intensity decreases, and the difference between the peak and valley of the magnetic induction intensity decreases.

The cross-sectional magnetic induction intensity in the vertical direction shown in Fig. 5 presents a symmetrical distribution that first increases and then decreases from the center to the outside. To simplify the problem, the magnetic field of each surface can be divided into a series of concentric rings. When the height from the bottom wall of the container is less than 6 mm, the difference between

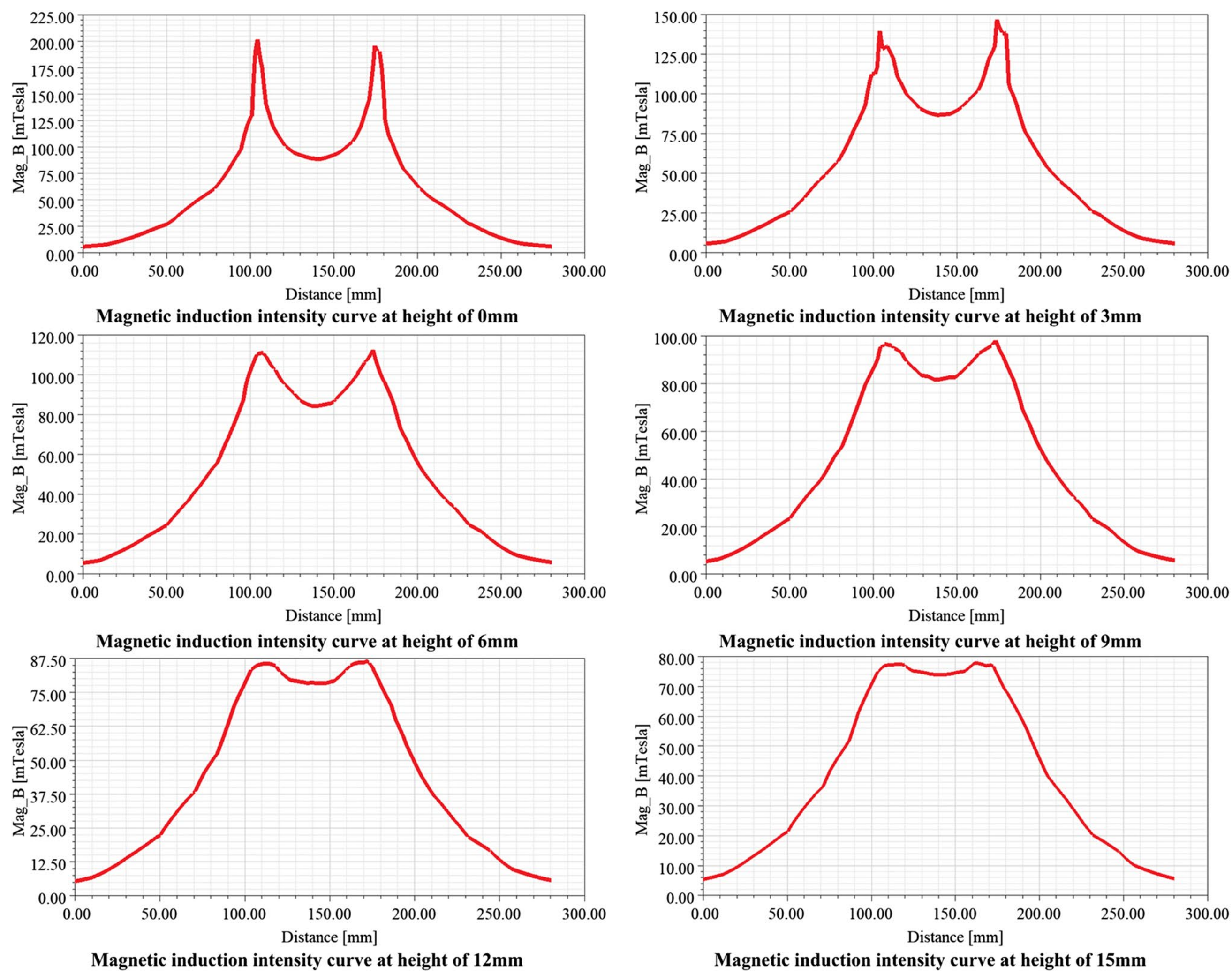

Fig. 5 Simulation results of electromagnet field

the maximum magnetic induction intensity and the central magnetic induction intensity is significant. Therefore, the region between the two values is divided into four rings, and the other regions are divided into two rings, for a total of 6 areas. When the height is greater than 6 mm, the difference in the central area is slight, and the magnetic field is evenly divided into six rings. The magnetic field divisions at heights of 0 mm and 9 mm are shown in Fig. 6a and b. The entire

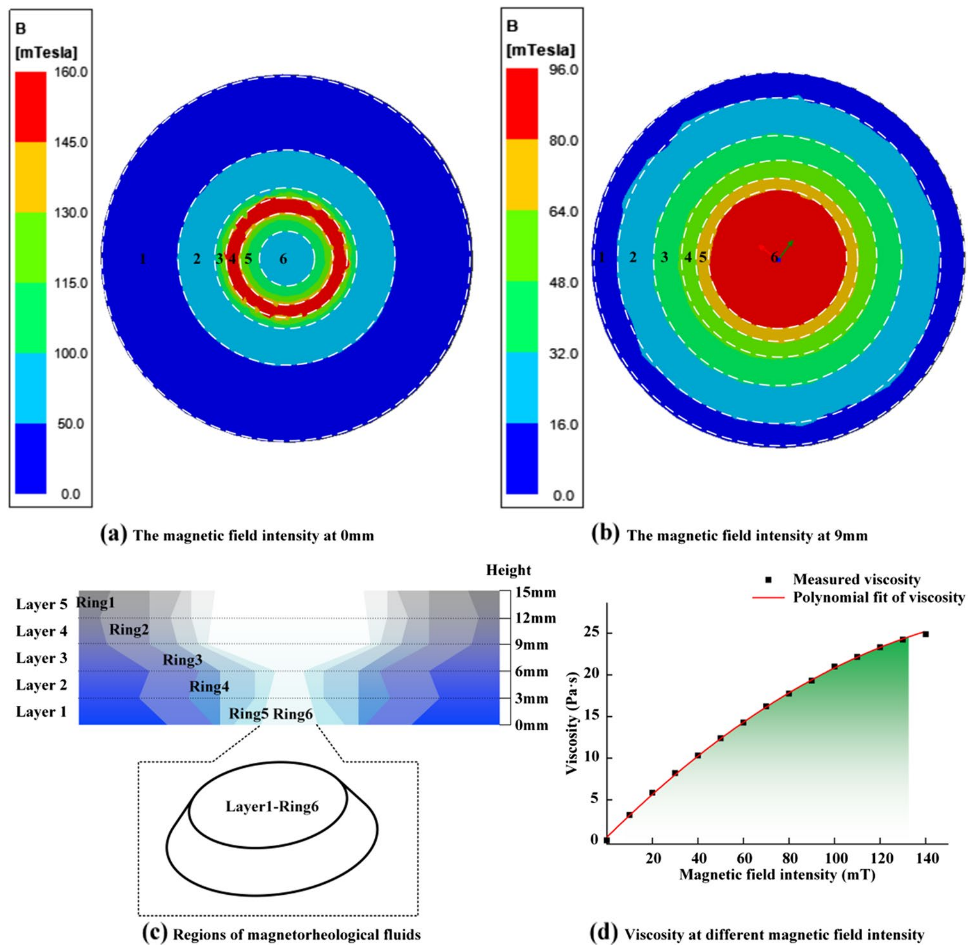

Fig. 6 The division of the magnetic field

Table 4 Zoning data for fluid simulation

Layer no	Parameters	Ring1	Ring2	Ring3	Ring4	Ring5	Ring6
1	Lower surface radius (mm)	120–70	70–44	44–40	40–32	32–16	16–0
	Upper surface radius (mm)	120–86	86–58	58–40	40–20	20–12	12–0
	Average intensity (mT)	20	57	104	133.5	96.5	86.5
2	Lower surface radius (mm)	120–86	86–58	58–40	40–20	20–12	12–0
	Upper surface radius (mm)	120–80	80–52	52–40	40–20	20–8	8–0
	Average intensity (mT)	16.5	42	84	107.5	90	84
3	Lower surface radius (mm)	120–80	80–52	52–40	40–20	20–8	8–0
	Upper surface radius (mm)	120–104	104–80	80–64	64–52	52–46	46–0
	Average intensity (mT)	13.5	34	61.5	77.5	82	86.5
4	Lower surface radius (mm)	120–104	104–80	80–64	64–52	52–46	46–0
	Upper surface radius (mm)	120–108	108–80	80–68	68–56	56–44	44–0
	Average intensity (mT)	8.5	24	36.5	52	67	83.5
5	Lower surface radius (mm)	120–108	108–80	80–68	68–56	56–44	44–0
	Upper surface radius (mm)	120–102	102–80	80–62	62–56	56–42	42–0
	Average intensity (mT)	7.5	19	31.5	45.5	61	74.5

magnetorheological fluid zone is divided into five layers, each layer is divided into six rings, and each zone resembles a frustum. The overall division is shown in Fig. 6c. Each zone's average magnetic induction intensity between two surfaces with a distance of 3 mm in the vertical direction is calculated as the actual magnetic field in that zone. The ring diameter and average magnetic induction intensity of each zone are shown in Table 4.

The relationship between the viscosity and the magnetic induction intensity is shown in Fig. 6d. With increasing magnetic induction intensity, the viscosity of the magnetorheological preparation fluid increases, but the growth rate decreases. Studies have shown that when the magnetic induction intensity is sufficiently large, the viscosity of the magnetorheological preparation fluid infinitely approaches a constant value. The off-state viscosity of the rheological fluid is 0.13 Pa·s. When the magnetic induction intensity is 140 mT, the fluid viscosity curve does not show a clear flattening trend, indicating that the magnetic field saturation has not been reached. However, since the maximum magnetic induction intensity of the zone in this study is 133.5 mT, it is unnecessary to continue increasing the magnetic induction intensity. The corresponding fluid viscosity can be obtained for the average magnetic induction intensity listed in Table 4. A fluid simulation model with variable viscosity under the influence of a magnetic field can be established by assigning the viscosity value to the fluid in each zone.

3.2 Material removal rate of the tool edge

3.2.1 Simulation results

Theoretically, the viscosity of the MR fluid increases with the increasing magnetic induction intensity, and the shear force on the cutting edge also increases, which can improve the preparation efficiency. Consequently, we placed the tool edge in a position with a larger magnetic induction intensity, as shown in Fig. 7, to obtain a significant change in edge shape in a shorter experimental time. Employing the established variable viscosity model, the flow field of the MR fluid in the grinding basin is simulated. The inlet flow rate is 10 m/s, and the cutting tool rotates counterclockwise at 360 r/min.

Taking the intersection of the rotation center axis and the tool edge as point o, an observation point is established every 1.5 mm, and the distribution of 6 observation points is shown in Fig. 7. Every 360 degrees of rotation is a cycle, and each point's dynamic pressure and relative velocity values at different angles are extracted. The P_dV fitting curves are shown in Fig. 8.

Considering the effect of the magnetic field on the viscosity, the fluid flow velocity decreases significantly with increasing viscosity. From point a to point f, the difference between the average relative velocity and linear speed continues to increase, reflecting the increasing trend of the fluid flow velocity. However, there is no strict quantitative relationship between the increase in relative velocity and the increase in linear velocity, indicating no clear pattern to follow for the increase in liquid flow rate. In a cycle, the P_dV value of each point does not change much, and the fitted curve is relatively flat. But when the rotation angle is about 240°, the value has a clear downward trend, mainly due to the lower relative velocity at this location. The further away from the center of rotation, the larger the P_dV value. It is primarily because the relative velocity of the observation points increases as the distance from the center of rotation increases, while the hydrodynamic pressure does not fluctuate much. At this time, the relative velocity becomes the decisive factor affecting the material removal rate of the cutting-edge preparation. The shaded area is the value of a single cycle for a point. Assuming that the fitting curve expression is $f(x)$, the area can be obtained by Eq. (5).

$$\sum_{P_dV} = \int_0^{2\pi} f(\times)dx \tag{5}$$

When the Preston coefficient and preparation time are the same, a larger P_dV value indicates a higher material removal rate. Therefore, when the tool is installed according to the position shown in Fig. 8, the material removal

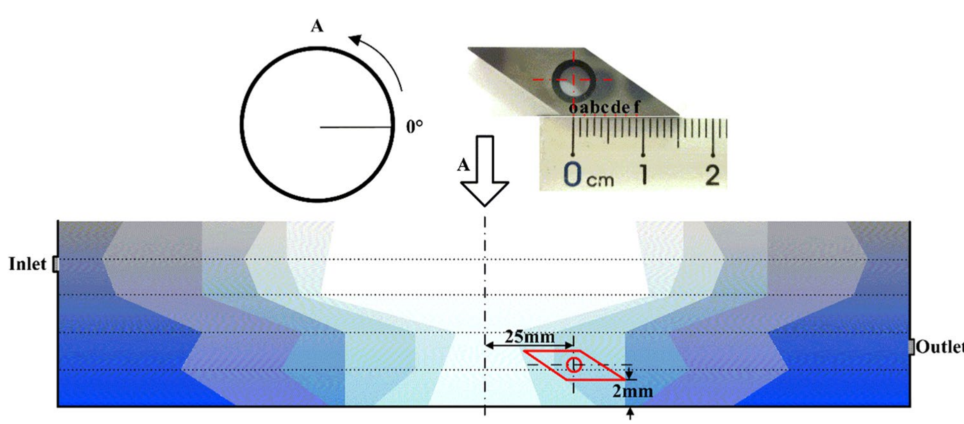

Fig. 7 Flow field simulation diagram

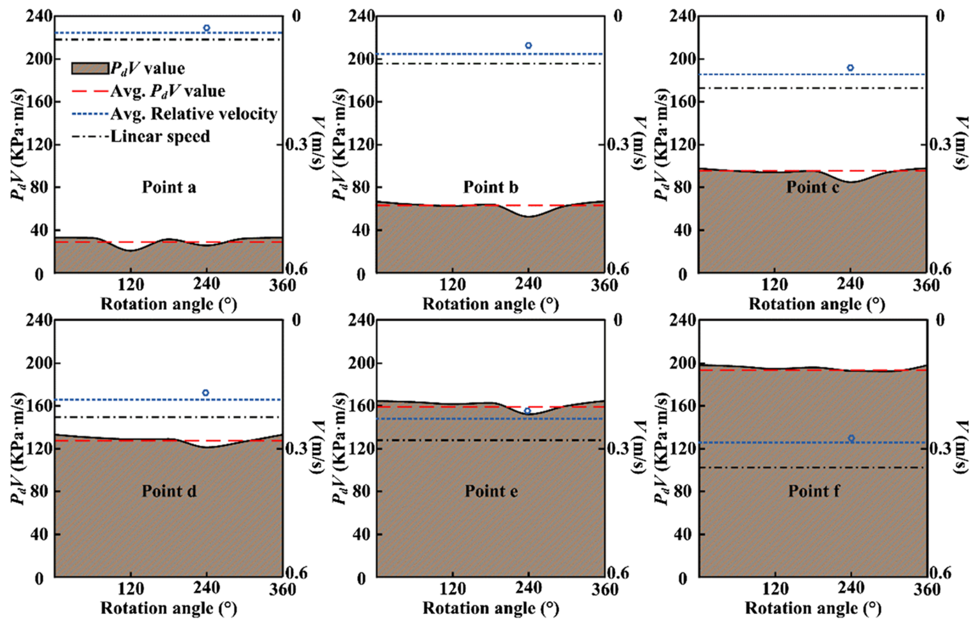

Fig. 8 The fitting curve of the P_dV value at each point

Table 5 Parameters of preparation experiment

Speed (r/min)	Tool material	Abrasive materials	Solid–liquid ratio	Preparation time (min)
360	Cemented carbide (K30)	Diamond powder W100	4:9	60

rate of each point on the cutting edge is different and gradually increases from point a to point f. At this time, the prepared cutting edge has non-uniform characteristics.

3.2.2 Experimental verification

The preparation experiments of cemented carbide cutting tools were carried out using the developed magnetorheological device to verify the simulation results. The parameters of the preparation experiment are shown in Table 5. The prepared tool edge was measured with a Keyence VK-X100 laser scanning confocal microscope (LSCM).

Before and after the preparation, the cutting edge was measured. Since the installation center is the symmetry center of the theoretical wedge angle during tool measurement, the maximum value of the relative height data on the cutting-edge section is extracted as the middle point. The transition points are identified using the approach presented in the literature [28]. Then, several height values on the left and right sides are taken as the input for edge fitting. MATLAB was employed to denoise and fit the cutting-edge height data, and the radius of the round cutting edge was obtained. The topography of the cutting edge before and after preparation is shown in Fig. 9. The comparison of cutting-edge profiles is shown in Fig. 10.

The edge radius change can be used as the evaluation index for the preparation effect. The real removal rate of

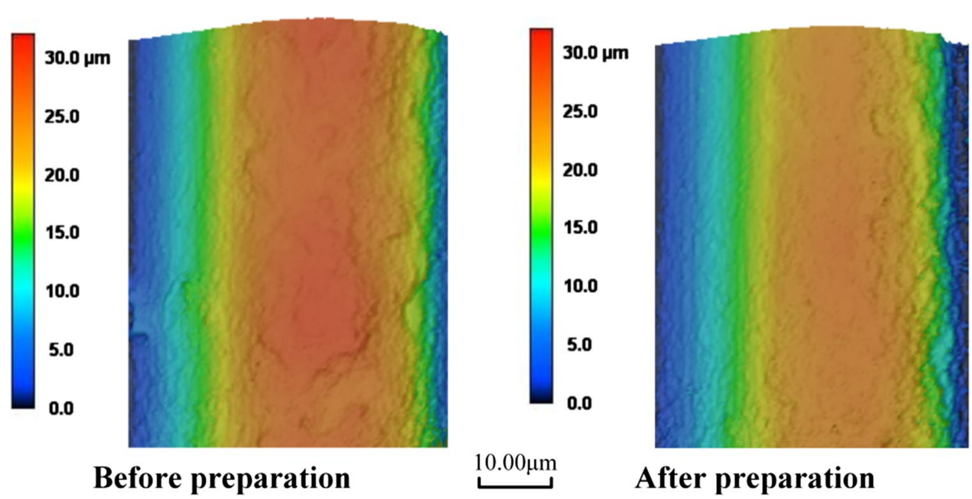

Fig. 9 Topography of cutting edge before and after preparation

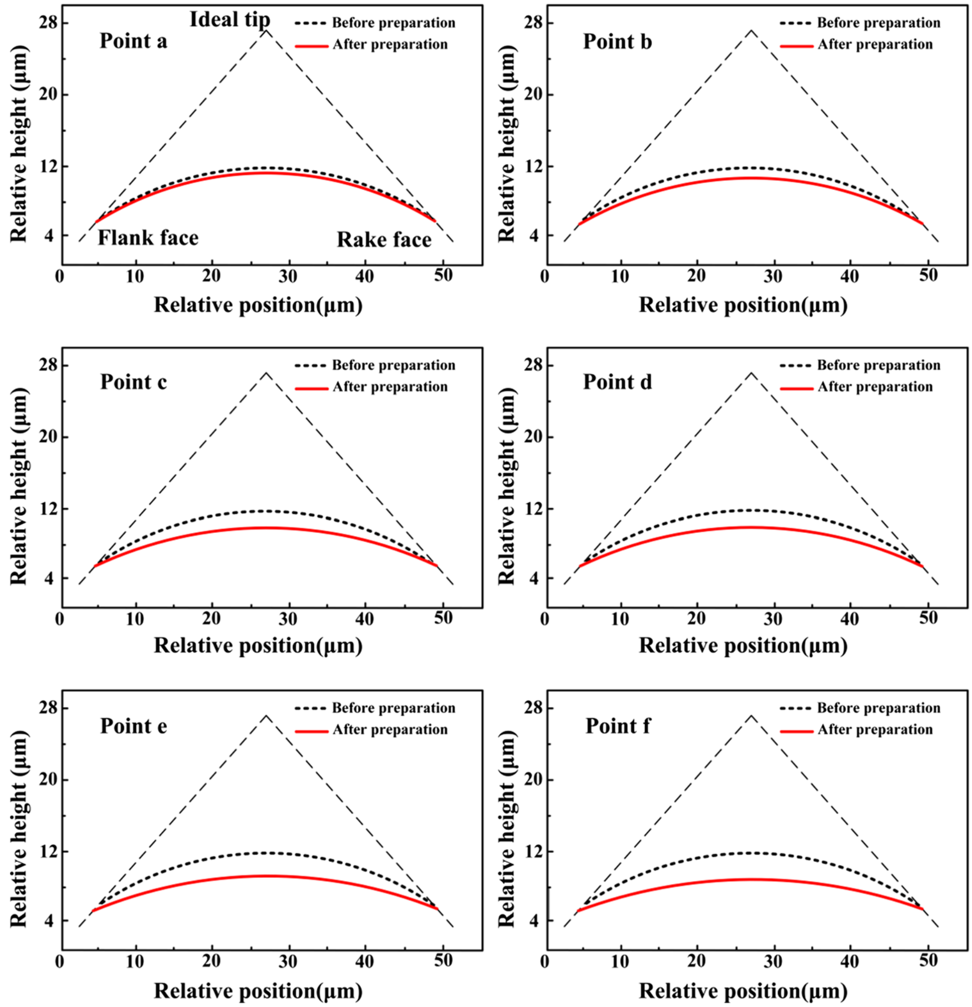

Fig. 10 Comparison of cutting-edge profiles

materials from point *a* to point *f* during the experiment can be obtained through precise measurement and data post-processing.

Figure 11 shows the P_dV variation curve obtained by simulation and the edge radius variation curve obtained by experiment. From point a to point f, the radius of the cutting edge increases gradually, and the material removal rate of the cutting edge shows an increasing trend, which is consistent with the variation of P_dV. According to the Preston equation, when the MR fluid and preparation time are the same, the removal of cutting-edge material is determined by the product of hydrodynamic pressure and relative velocity. Therefore, the experimental results verify the correctness of the simulation. The maximum change in the cutting-edge radius is used to characterize the cutting-edge removal rate, and the Preston coefficient of the magnetorheological fluid under the process conditions can be calculated. From point a to point f, the K value fluctuates slightly, the minimum value is 3.55E-15 m^2/N, and the maximum value is 4.16E-15 m^2/N, which appear at points *b* and *e* respectively. However, the standard deviation of K is about 2.01E-16 m^2/N, and the average value of K is 3.91E-15 m^2/N, which is smaller than the values measured in other studies [29, 30]. It may be due to the lower relative rotational speed and the smaller magnetic induction intensity. A smaller value of K means that the removal efficiency of preparation is low. Consequently, to increase the cutting-edge material removal rate in practical applications, increasing the rotational speed of the cutter bar may be considered. Alternatively, a preparation process combining brush and magnetorheological approach can be used to achieve low-damage customized removal to ensure preparation efficiency.

3.3 Effect of the installation position on the cutting-edge material removal rate

The above study shows that in the zone with the highest magnetic induction intensity, the tool edge's material removal rate increases gradually from the center of rotation to the outside as the relative speed increases. The prepared edge radius shows a non-uniform "small to large" characteristic. To investigate the distribution of the removal rate in the rest zones, the tools were placed at different

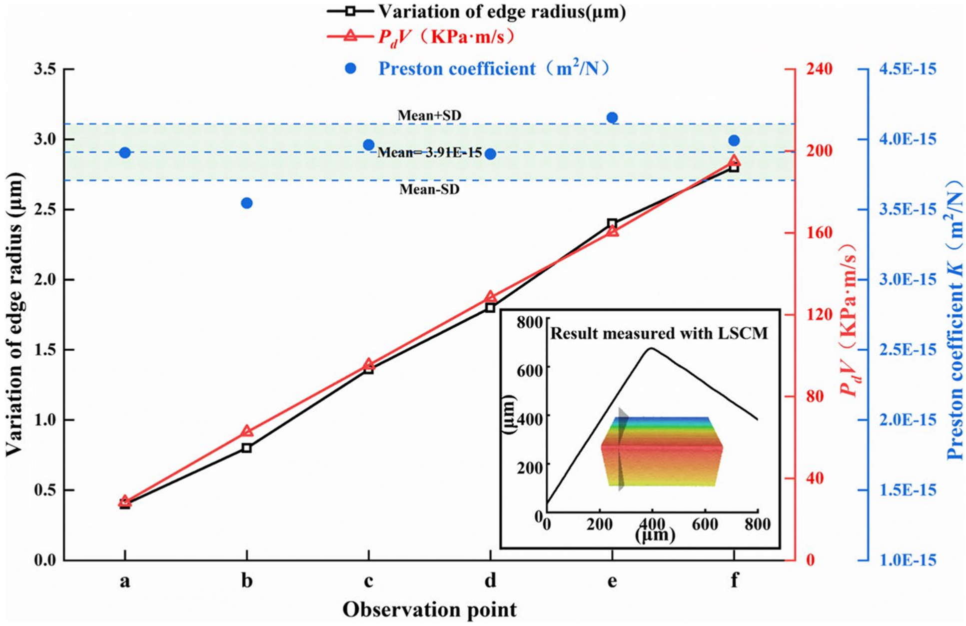

Fig. 11 The material removal rate and Preston coefficient

positions in the plane of 2 mm and 7 mm from the bottom of the grinding basin. The simulation study of the P_dV value was conducted, and the results are shown in Fig. 12.

The P_dV values from the center of rotation outward at different positions show a gradually increasing trend, but in zones I and VI near the basin wall, the changes in the P_dV values are complex. As zone VI is close to the outlet, the fluctuation range of the P_dV value is more obvious than that of zones I. It shows that the average value of P_dV from point *a* to *f* does not show apparent regularity due to the complex flow state of the wall effect, and the P_dV fluctuates greatly when each point rotates to different angles. Therefore, placing the

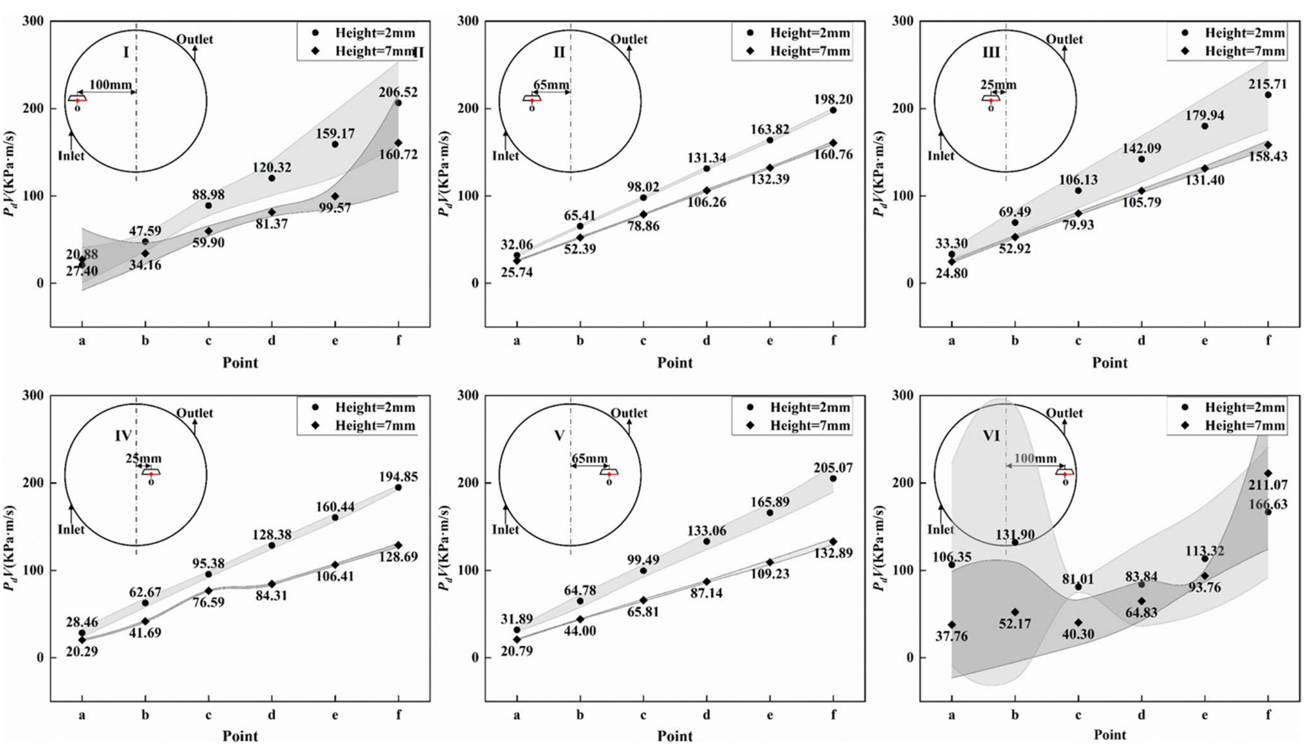

Fig. 12 Simulation results of P_dV values

tool close to the basin wall should be avoided when preparing the tool edge. In the zone away from the wall, the P_dV value at each point shows a linear change, and the changing trend is consistent with the evolution of the rotation speed of each point, indicating that the relative speed plays a decisive role.

When the left and right positions are the same, the further away from the basin floor, the smaller the P_dV value as the magnetic induction intensity decreases. Bingham fluid shear is weakened, and edge material removal efficiency is reduced. However, at the height of 7 mm from the bottom surface, the standard deviation of P_dV values from points a to f at different rotation angles in zones II–V is smaller than that at the height of 2 mm, reflecting better uniformity of the flow field here. At the height of 2 mm from the bottom surface, the mean value of P_dV at each point in zone IV is the smallest, and the mean value of P_dV at each point in zone III is the largest, with the latter being 1.11–1.17 times that of the former. The P_dV values of a to f in regions II–V have a strong linear relationship, but the slopes of the fitted straight lines are slightly different. The slope of zone 3 is the largest, and the slope of zone 4 is the smallest. The fluid viscosity in region III and region IV is the same, but region III is closer to the inlet than region IV, and its removal rate is greater than that of the latter. The cutting-edge material removal rate is not simply proportional to the viscosity. The distance between the cutting edge and the magnetic field generator should be minimized to improve the material removal rate when using the presented approach to prepare the cutting edge. At the same time, the edge material removal efficiency and distribution characteristics are influenced by the tool bar rotation speed in addition to the position of the tool in the basin. The preparation requirements for non-uniform edges can be met for particular edges by adjusting the tool-mounting angle and position in the basin.

4 Conclusion

(1). The differential removal mechanism of cutting-edge material based on magnetorheological finishing is discussed, and the feasibility of achieving non-uniform preparation of cutting edge is verified by simulation and experimental. It provides a simple, low-cost method for accurate and low-damage preparation of non-uniform edges.

(2). A magnetorheological preparation device was built, and the structure of the grinding basin was optimized. The round-shaped basin with different sides and height openings was employed to reduce the low-speed flow region and facilitate the adequate flow of magnetorheological fluid.

(3). The magnetic induction intensity distribution law is studied, and the results show that the magnetic induction intensity has an “M” shape distribution. From the edge to the center of the container, the magnetic induction intensity first increases and then decreases and is symmetric around the axis. The magnetic induction intensity reaches a maximum at about 35 mm from the center. With increasing height, the magnetic induction intensity’s peak decreases, and the magnetic induction intensity’s peak-valley difference decreases. The flow field simulation model with variable viscosity is established, which helps achieve a high-precision flow field simulation.

(4). The flow field simulation shows that in the zone with the largest fluid viscosity, the P_dV value of each point on the cutting-edge increases with increasing rotation speed, and the edge material removal rate is non-uniform. The fitted cutting-edge radius change value is used to characterize the cutting-edge removal amount, and the Preston coefficient can also be calculated. It provides a basis for studying the material removal law of similar magnetorheological preparation fluids. However, due to the limitation of container size and rotation speed, the material removal rate is relatively low and equipment optimization and process improvement can be considered later to improve the material removal rate.

(5). P_dV of the tool located in the different zones were studied. The results showed that the edge material removal efficiency and distribution characteristics were affected by the rotation speed of the tool and related to the position in the basin. In this paper, the cutting edge’s material removal rate increases gradually from the center of rotation to the outside, and the radius of the prepared cutting-edge changes from “small to large.” By redesigning the cutter bar clamping mechanism and adjusting the tool installation position, it is possible to prepare non-uniform edges such as “large to small” and “large in the middle and small at the ends.”

Author contribution Xiangyu Guan: validation, investigation, writing—original draft; Donghai Zhao: investigation, writing—original draft; Yaxin Yu: data curation, software, validation; Dunwen Zuo: conceptualization, supervision; Shuquan Song: conceptualization, methodology, supervision, writing—original draft.

Funding The study was funded by the National Natural Science Foundation of China (No.51605414), the Postgraduate Research and Practice Innovation Project of Yancheng Institute of Technology (SJCX21_XZ004, SJCX22_XZ017, SJCX22_XY034), and the Key Laboratory Fund Project of Zhejiang Provincial Key Laboratory for Cutting Tools (ZD202110).

Data availability Data related to this work will be provided upon request.

Code availability Part of the code can be provided upon request for noncommercial purpose.

Declarations

Ethics approval The manuscript has only been communicated to one journal only and has not been submitted to more than one journal for simultaneous consideration.

Consent to participate The authors have given their consent to participate.

Consent for publication The authors have given their consent to publish the present paper.

Conflict of interest The authors declare no competing interests.

References

1. Uysal A, Ozturk S, Altan E (2015) An experimental study on dead metal zone in orthogonal cutting with worn rounded-edge cutting tools. Int J Mater Prod Technol 51(4):401–412
2. Woon KS, Chaudhari A, Rahman M, Wan S, Kumar AS (2014) The effects of tool edge radius on drill deflection and hole misalignment in deep hole gun drilling of Inconel-718. CIRP Ann 63(1):125–128
3. Denkena B, Grove T, Maiss O (2015) Influence of the cutting edge radius on surface integrity in hard turning of roller bearing inner rings. Prod Eng Res Devel 9(3):299–305
4. Vopát T, Sahul M, Haršáni M, Vortel O, Zlámal T (2020) The tool life and coating-substrate adhesion of AlCrSiN-coated carbide cutting tools prepared by LARC with respect to the edge preparation and surface finishing. Micromachines 11(2):166
5. Zhao T, Agmell M, Persson J, Bushlya V, Ståhl JE, Zhou JM (2017) Correlation between edge radius of the cBN cutting tool and surface quality in hard turning. J Superhard Mater 39(4):251–258
6. Hariprasad B, Selvakumar SJ, Raj DS (2022) Effect of cutting edge radius on end milling Ti–6Al–4V under minimum quantity cooling lubrication–chip morphology and surface integrity study. Wear 498:204307
7. Jiang F, Guo B, Liao T, Wang FZ, Cheng X, Yan L, Xie H (2019) Optimizing the geometric parameters of cutting edge for the finishing machining of 30Cr alloy steel. Int J Comput Methods 16(08):1850117
8. An QL, Ming WW, Cai XJ, Chen M (2015) Effects of tool parameters on cutting force in orthogonal machining of T700/LT03A unidirectional carbon fiber reinforced polymer laminates. J Reinf Plast Compos 34(7):591–602
9. Bouzakis KD, Charalampous P, Kotsanis T, Skordaris G, Bouzakis E, Denkena B, Breidenstein B, Aurich JC, Zimmermann M, Herrmann T, M'saoubi R (2017) Effect of HM substrates' cutting edge roundness manufactured by laser machining and micro-blasting on the coated tools' cutting performance. CIRP J Manuf Sci Technol 18:188–197
10. Zimmermann M, Kirsch B, Kang YY, Herrmann T, Aurich JC (2020) Influence of the laser parameters on the cutting edge preparation and the performance of cemented carbide indexable inserts. J Manuf Process 58:845–856
11. Na Y, Lee US, Kim BH (2021) Experimental study on micro-grinding of ceramics for micro-structuring. Appl Sci 11(17):8119
12. Oliaei SNB, Karpat Y (2016) Investigating the influence of built-up edge on forces and surface roughness in micro scale orthogonal machining of titanium alloy Ti6Al4V. J Mater Process Technol 235:28–40
13. Krebs E, Wolf M, Biermann D, Tillmann W, Stangier D (2018) High-quality cutting edge preparation of micromilling tools using wet abrasive jet machining process. Prod Eng Res Devel 12(1):45–51
14. Wang WT, Biermann D, Aßmuth R, Arif AFM, Veldhuis SC (2020) Effects on tool performance of cutting edge prepared by pressurized air wet abrasive jet machining (PAWAJM). J Mater Process Technol 277:116456
15. Tiffe M, Aßmuth R, Saelzer J, Biermann D (2019) Investigation on cutting edge preparation and FEM assisted optimization of the cutting edge micro shape for machining of nickel-base alloy. Prod Eng Res Devel 13(3):459–467
16. Denkena B, de León L, Bassett E, Rehe M (2010) Cutting edge preparation by means of abrasive brushing. Key Eng Mater 438:1–7
17. Malkorra I, Souli H, Claudin C, Salvatore F, Arrazola P, Rech J, Seux H, Mathis A, Rolet J (2021) Identification of interaction mechanisms during drag finishing by means of an original macroscopic numerical model. Int J Mach Tools Manuf 168:103779
18. Lv D, Wang YG, Yu X, Chen H, Gao Y (2022) Analysis of abrasives on cutting edge preparation by drag finishing. Int J Adv Manuf Technol 119(5):3583–3594
19. Karpuschewski B, Byelyayev O, Maiboroda VS (2009) Magneto-abrasive machining for the mechanical preparation of high-speed steel twist drills. CIRP Ann 58(1):295–298
20. Endres WJ, Kountanya RK (2002) The effects of corner radius and edge radius on tool flank wear. J Manuf Process 4(2):89–96
21. Ducobu F, Rivière-Lorphèvre E, Filippi E (2017) Experimental and numerical investigation of the uncut chip thickness reduction in Ti6Al4V orthogonal cutting. Meccanica 52(7):1577–1592
22. Abdellaoui L, Khlifi H, Bouzid SW, Hamdi H (2020) Tool nose radius effects in turning process. Mach Sci Technol 25(1):1–30
23. Vipindas K, Anand KN, Mathew J (2018) Effect of cutting edge radius on micro end milling: force analysis, surface roughness, and chip formation. Int J Adv Manuf Technol 97(1):711–722
24. Yussefian NZ, Hosseini A, Hosseinkhani K, Kishawy HA (2017) Design for manufacturing of variable microgeometry cutting tools. J Manuf Sci Eng 140(1):011014
25. Özel T (2009) Computational modelling of 3D turning: influence of edge micro-geometry on forces, stresses, friction and tool wear in PcBN tooling. J Mater Process Technol 209(11):5167–5177
26. Karpat Y, Özel T, Sockman J, Shaffer W (2007) Design and analysis of variable micro-geometry tooling for machining using 3-D process simulations. In: Proceedings of International Conference on Smart Machining Systems
27. Peng XQ (2004) Research on key technologies of deterministic magnetorheological polishing. Dissertation, National University of Defense Technology
28. Song SQ, Lu B, Zuo DW, Zhou H, Zhen L, Zhou F (2020) A new cutting edge surface reconstruction method for hard whirling tools. Meas 151:107276
29. Peng XQ, Dai YF, Li SY (2004) Mathematical model of material removal in magnetorheological polishing. Chin J Mech Eng 40(4):67–70
30. Xu J (2015) Research on magnetorheological polishing process and polishing trajectory of small tool head. Dissertation, Harbin Institute of Technology